Bonding Mechanisms in Resistance Microwelding of 316 Low-Carbon Vacuum Melted Stainless Steel Wires

M.I. KHAN, J.M. KIM, M.L. KUNTZ, and Y. ZHOU

Resistance microwelding (RMW) is an important joining process used in the fabrication of miniature instruments, such as electrical and medical devices. The excellent corrosion resistance of 316 low-carbon vacuum melted (LVM) stainless steel (SS) wire makes it ideal for biomedical applications. The current study examines the microstructure and mechanical properties of crossed resistance microwelded 316LVM wire. Microtensile and microhardness testing was used to analyze the mechanical performance of welds, and fracture surfaces were examined using scanning electron microscopy. Finally, a bonding mechanism is proposed based on optimum joint breaking force (JBF) using metallurgical observations of weld cross sections. Moreover, comparisons with RMWs of Ni, Au-plated Ni, and SUS304 SS wire are discussed.

DOI: 10.1007/s11661-009-9780-x

I. INTRODUCTION

EXCELLENT corrosion resistance coupled with nonmagnetic properties has made austenitic stainless steel (SS) ideal for implantable medical devices.[1] In particular, 316 low-carbon vacuum melted (LVM) wire has been used in medical instruments for several decades. Various welding processes[2,3] have been used to fabricate these components; however, limited literature exists on microwelding of austenitic SS used in medical devices.[1,4]

Resistance welding has been widely used in the electrical and medical industries, because it is an economical process that offers improved productivity and equipment costs compared to laser welding. Medical devices are miniature and integrated, which results in a reduction of scale in joint size from millimeters (mm) to micrometers (μm) in such applications including, but not limited to, biosensors, stents, catheters, pacemakers, and surgical instruments.[5] Miniature resistance welding is commonly known as small-scale resistance spot welding and is often referred to as resistance microwelding (RMW).

The RMW of Ni sheet, Ni wire, and Au-plated Ni wire has previously been investigated.[6–8] Fukumoto *et al.*[7] described the weld development and bonding mechanism for pure Ni wire by incrementally increasing the weld current. Solid-state bonding produced the optimum joint breaking force (JBF). In the case of Au-plated Ni wire, the optimized bonding mechanism of RMW was a combination of solid-state bonding, brazing, and fusion welding.[8]

Recently, Fukumoto *et al.*[1] investigated RMW of SUS304 SS wire, which is an austenitic SS. Solid-state bonding was again suggested over fusion welding at the optimum JBF. However, the RMW bonding mechanism of 316 LVM SS is not fully understood. The objective of this study is to detail the bonding mechanism of 316LVM SS through experimental development and to compare the joint formation and mechanical properties with previous studies on RMW of crossed wires.

II. EXPERIMENTAL PROCEDURES

A. *Machine Setup and Welding Parameters*

The chemical composition for the 0.015-in.- (0.38-mm-) diameter 316 LVM SS wire (New England Precision Grinding, Inc., Holliston, MA) is shown in Table I. Before bonding, all samples were ultrasonically cleaned in acetone. Figure 1(a) shows a schematic of the wire dimensions and joint configuration, in which wires were bonded at right angles (90 deg). A MacGregor DC400P direct-current controller and Unitek 80A/115 V weld head (Miyachi Unitek Corporation, Monrovia, CA) were used. Flat-ended, round RWMA class 2 (Cu-Cr) electrodes with a 3.2-mm face diameter were used to apply force and current. Two electrode force levels were used, including 1.5 and 5 kg-f. The current was varied between 90 and 350 A and applied for a total weld time of 50 ms including an up-slope time of 10 ms and a down-slope time of 3 ms.

B. *Microstructure and Mechanical Properties*

The JBF was determined using an Instron model 5548 microtensile tester (Instron, Norwood, MA). A 500 N load cell with an accuracy of $\pm$0.4 pct was used with a crosshead speed of 10 mm/min. Weld cross sections were observed using optical microscopy, and scanning electron microscopy was used to examine fracture

M.I. KHAN and J.M. KIM, Students, M.L. KUNTZ, Research Assistant, and Y. ZHOU, Professor, are with the Department of Mechanical & Mechatronics Engineering, Centre for Advanced Materials Joining, University of Waterloo, Waterloo, ON, Canada N2L 3G1. Contact e-mail: ibraheem@rogers.com
Manuscript submitted March 7, 2008.
Article published online February 20, 2009

Table I. Chemical Composition of 316LVM Wire

	C	Mn	Si	P	S	Cr	Ni	Mo	Cu	N	Fe
Wt pct	0.024	1.84	0.75	0.017	<0.001	17.47	14.73	2.76	0.04	0.024	bal

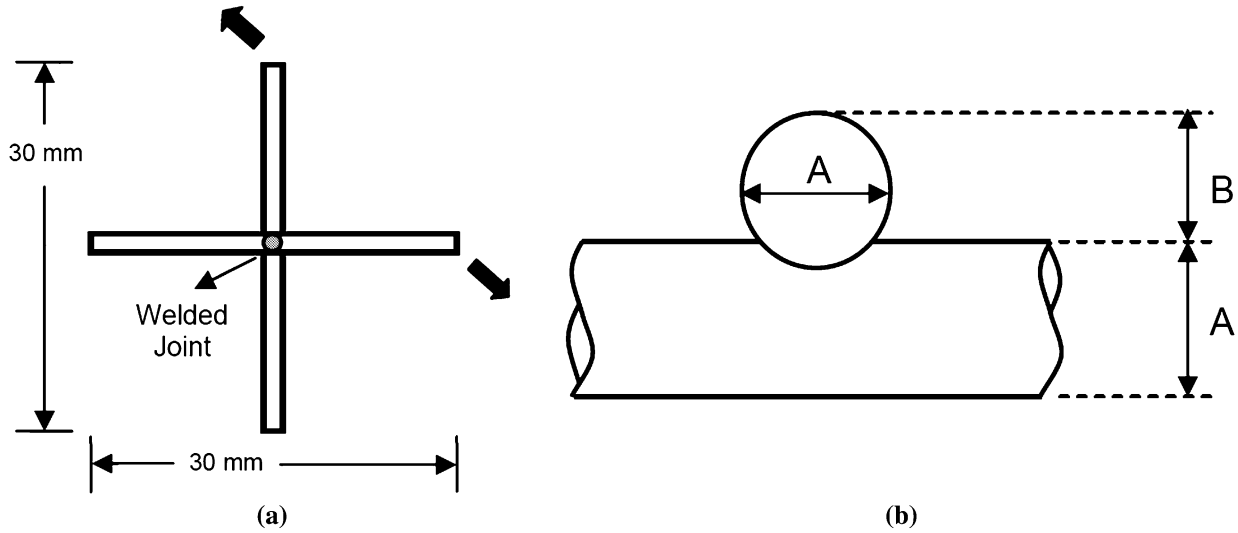

Fig. 1—Schematic of (*a*) tensile test and (*b*) set-down.

surfaces. Samples were etched with a solution of 5 mL HNO_3, 25 mL HCl, and 30 mL H_2O at an elevated temperature (80 °C) between 3 to 5 seconds depending on the bonding condition.

The joint collapse[9] was quantified by the set-down, which was calculated using Eq. [1]:

$$\text{Setdown (pct)} = \frac{A - B}{A} \times 100 \qquad [1]$$

where A is the diameter of wire and B is the resultant height of the joined wires less the initial wire diameter A, as shown in Figure 1(b). A Wyko NT1100 optical profiler (Veeco Instruments Co., Plainview, NY) was used to accurately measure parameters A and B. Hardness testing was conducted on a Shimadzu microhardness tester (Shimadzu Corporation, Kyoto, Japan) with a 10-g load held for 15 seconds.

III. EXPERIMENTAL RESULTS

A. *Microstructure of Welded Joints*

The cross sections of RMW joints produced at an electrode force of 1.5 kg-f over the current range of 54 to 350 A, including the absolute set-down values, are shown in Figure 2. At 54 A, there was insufficient heating at the faying surface to initiate bonding. Figure 2(a) shows some grain growth near the weld interface due to heat generated during the current on-time. Application of the electrode force (1.5 kg-f) resulted in slight set-down as the point contact between the crossed wires spread to a deformed contact patch. This initial stage was termed "stage 1" by Fukomoto and Zhou,[6] who observed "cold collapse" in RMW of Ni wires.

At a weld current of 90 A, melting of a thin surface film was observed ("stage 2"[7]). This layer melted first due to a high contact resistance. The molten layer was immediately squeezed out, taking some of the contaminants and oxides to the periphery, leaving behind a clean metallic surface ("stage 3").[7] The squeezed-out flash was visible near the edge of the interface (Figure 2(b)). The microstructure of the flash showed fine liquated grains, which suggested that the squeezed-out liquid layer was partially molten, or mushy. Liquated grains have been found in the heat-affected-zone of fusion-welded austenitic steels due to low melting point constituents, such as Si, P, and C, which segregated to the grain boundaries (GBs).[10,11] This was exasperated by grain growth, which decreases GB area and increases the concentration of impurities at GBs. For example, Kujanpaa *et al.*[12] found S enrichment at 2000 times the normal concentration in liquated GBs of 310 SS.

Increasing the current to 100 A resulted in an enlarged heat-affected zone (HAZ) around the interface, as shown in Figure 2(c), and triggered dynamic recrystallization of the fine-grained base metal microstructure. Liquated GBs at the faying surface interface were observed without any indication of a fully molten fusion zone. Thus, in the case of SS, initial bonding was facilitated by GB liquation. Continued set-down and recrystallization was also observed by Fukumoto and Zhou ("stage 4"),[7] who found that solid-state bonding was the mechanism of joint formation in RMW of Ni wires.

At weld currents above 120 A, there was formation and growth of a fusion zone. An increase in fusion zone diameter from nearly 30 μm to about 200 μm was

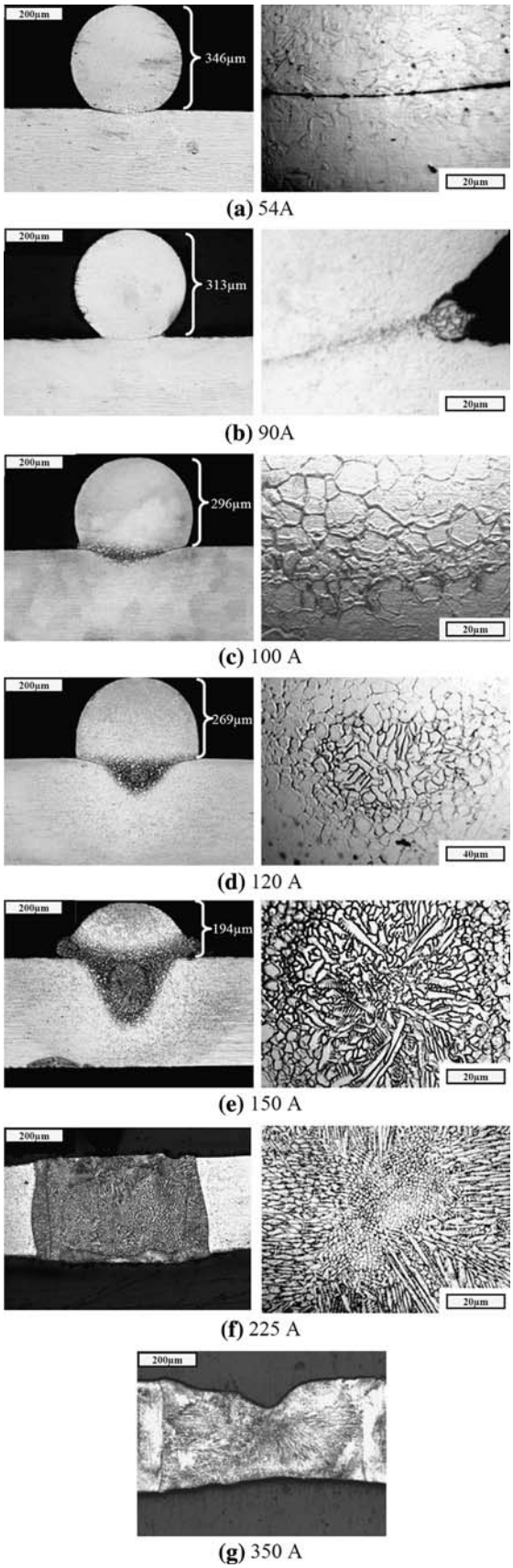

Fig. 2—Weld cross sections for RMW 316 LVM using 1.5 kg-f weld force.

observed in Figures 2(d) and (e), respectively. The high contact resistance resultant from low bonding force (1.5 kg-f) coupled with high electrical resistivity (740 $\mu\Omega$ mm) of the 316 LVM SS enabled peak temperatures to surpass the liquidus and form a dendritic solidification structure after rapid cooling. Given the chemical composition of 316 LVM SS (Table I), the expected solidification mode would be either austenite (A) or austenite-ferrite (AF), which are common to similar grades of austenitic SS.[11] Figure 2(e) shows that the solidification mode was predominantly austenitic (A).

Increasing the current to 225 A resulted in full fusion zone penetration and complete set-down, as shown in Figure 2(f). The formation of the fusion zone, or the proposed "5th stage" of bond development, was observed in RMW of 316 LVM SS wires but absent in Ni wires, likely due to the substantially higher electrical resistivity of 316 LVM SS. Overheating occurred when 350 A was applied, such that severe expulsion and deformation created the unacceptable weld profile shown in Figure 2(g).

B. *Relative Set-Down and JBF*

The effect of peak current on set-down is shown in Figure 3. There was an initial set-down of around 20 pct, called cold collapse, due to the applied force of 1.5 kg-f. A gradual increase in set-down, up to 40 pct, was observed as the current was increased to 150 A. Above 150 A, the set-down suddenly increased to 90 pct, which was attributed to the collapse of the wires upon melting. Complete set-down was attained with weld currents above 200 A, when full fusion occured.

The JBF as a function of current and the corresponding fracture modes are shown in Figure 4. A minimum weld current of 90 A was required to initiate bonding. It is likely that a requisite for bonding was the squeezing out of surface contaminants observed in Figure 2(b). There was a gradual increase in JBF between 90 and 200 A. The peak JBF of about 75 N was attained when

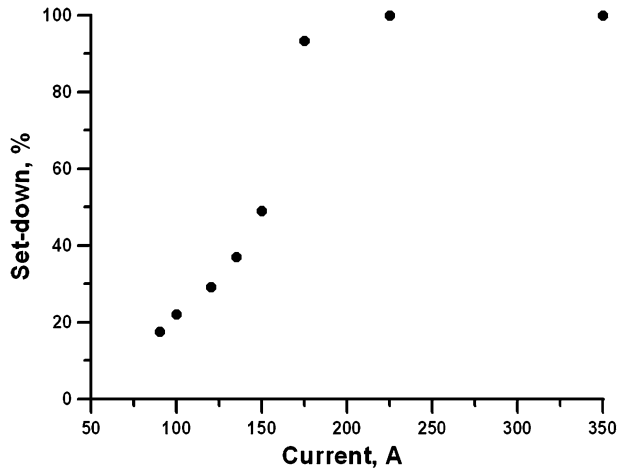

Fig. 3—Set-down as a function of RMW current for 316 LVM using 1.5 kg-f weld force.

the current exceeded 200 A. Overwelding occurred when the peak current surpassed 350 A. Metallographic observation of a weld cross section at the peak JBF current range (Figure 2(f)) showed full-fusion welding. Hence, the optimized bonding mechanism for maximum JBF can be described as full penetration fusion welding, where the entire cross section of wire melts and resolidifies. The surface tension of the liquid and the presence of the electrodes kept the liquid within the joint compared to the overwelding condition, where the fusion zone became too large and was subject to drop-through and thinning defects, which reduced the mechanical properties. Large variations in the JBF were observed for the optimal conditions, which has also been shown in past literature.[1,7,8] This scatter may be attributed to the nature of the tensile test setup, which inevitably resulted in combined loading conditions.

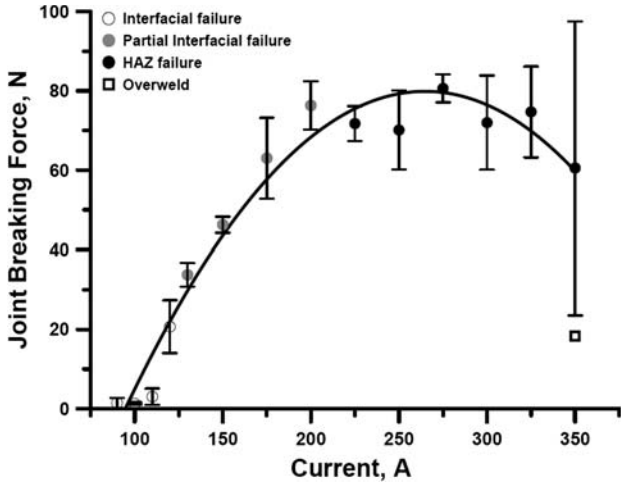

Fig. 4—JBF as a function of current for RMW 316LVM using 1.5 kg-f weld force.

C. *Fracture Surfaces*

Fracture surfaces of tensile samples are shown in Figures 5 through 7. Interfacial failure modes were observed for the 100 A welding condition (Figure 5). A small bonded region, about 150 μm in diameter, was evident at the center of the fracture surface. Dimples in this region are similar to those observed by Wang

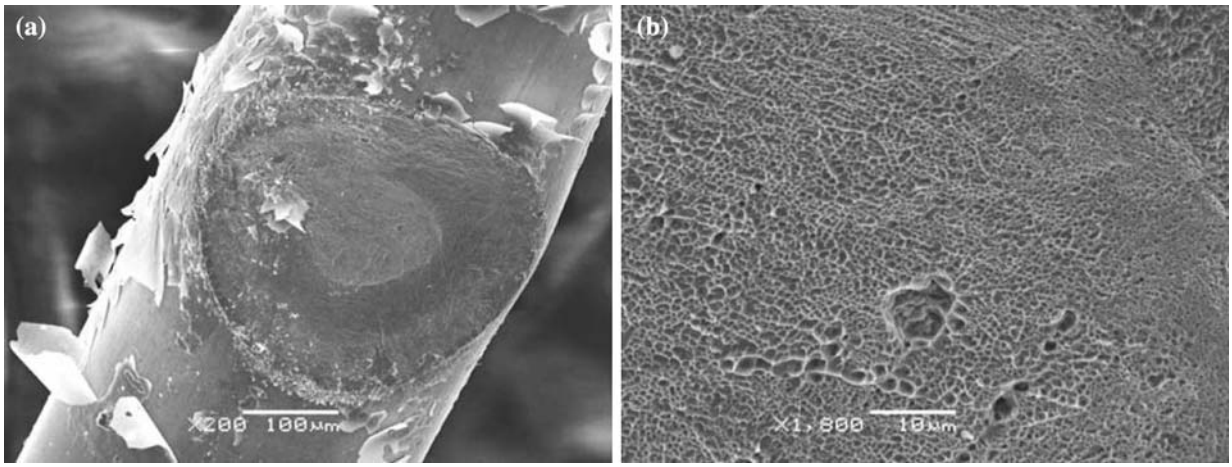

Fig. 5—Fracture surfaces for weld made using 100 A and 1.5 kg-f weld force.

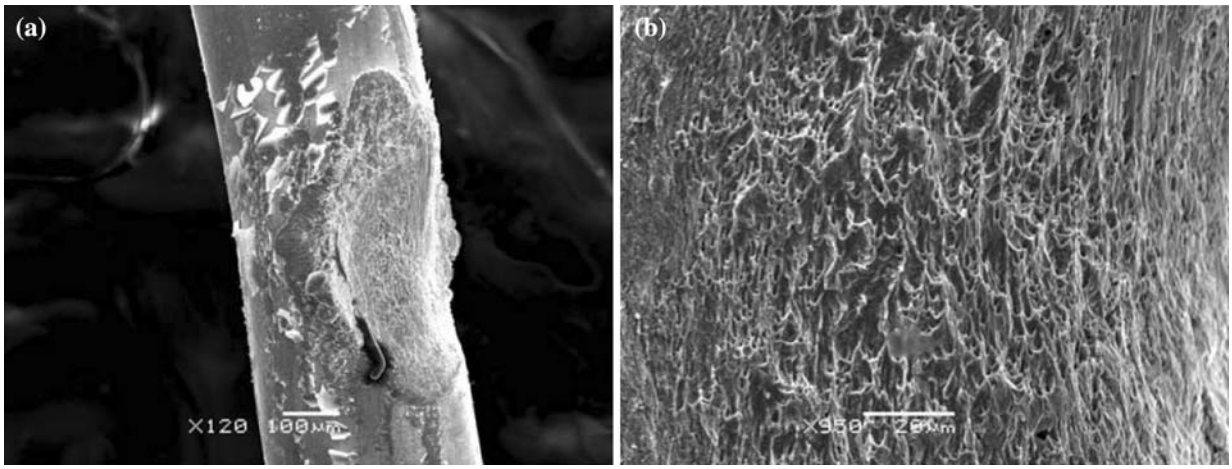

Fig. 6—Fracture surfaces for weld made using 120 A and 1.5 kg-f weld force.

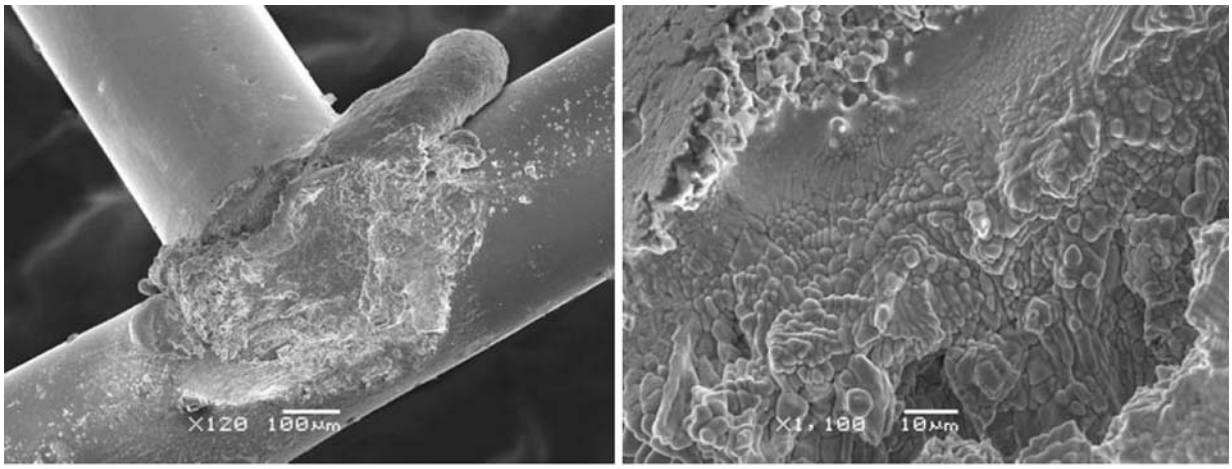

(a) 150 A

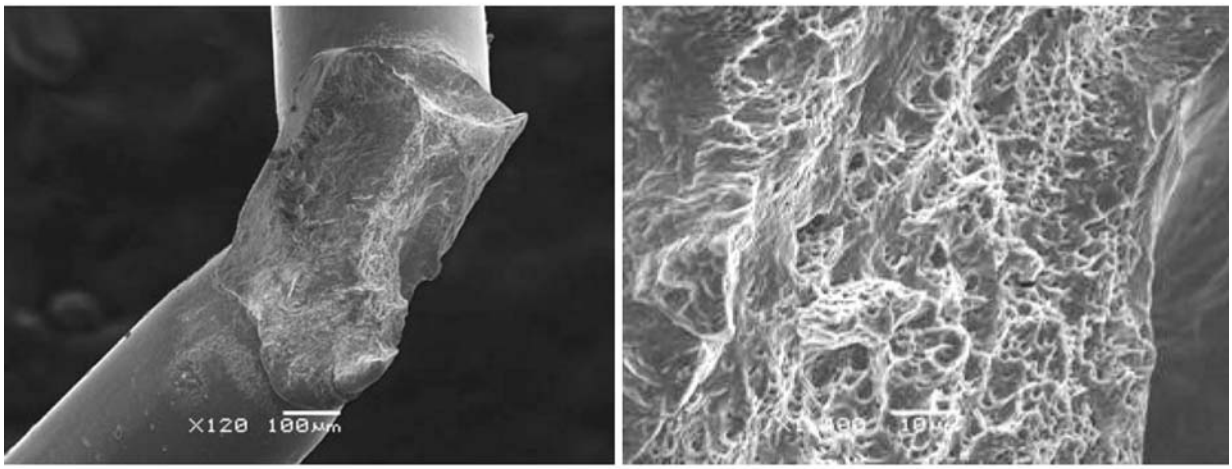

(b) 200 A

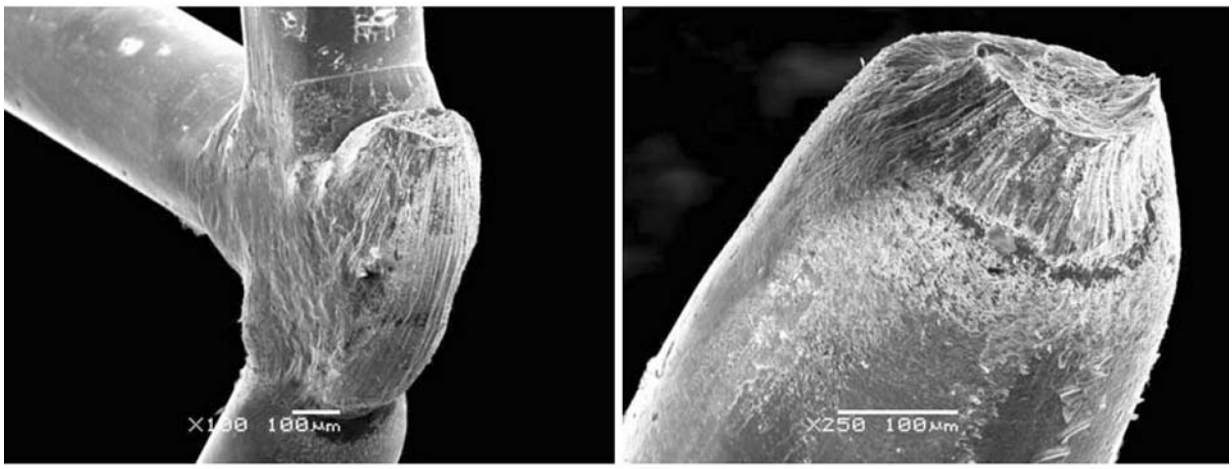

(c) 225 A

Fig. 7—Fracture surfaces showing transition to HAZ failure using 1.5 kg-f weld force.

et al.[13] for diffusion bonding. The periphery was deformed by cold collapse, showing an imprint of the opposite wire. Interfacial fracture was once again observed at 120 A, as shown in Figure 6. As compared to 100 A, the 120 A welding condition resulted in a larger bonded area, around 300 μm in diameter, which resulted in a higher JBF. Figure 6(b) shows the ductile dimpled fracture surface area in the center.

Fracture surfaces for 150, 200, and 225 A welding conditions are shown in Figure 7. As previously discussed, above 120 A, transition to a predominantly fusion bonding mechanism occurred. Similarly, the

failure mode also showed a transition from interfacial, to partial-interfacial, and finally, to HAZ failure. Figure 7(a) (150 A) shows the beginning of the transition toward partial interfacial failure, where fracture occurred near the interface. Figure 7(b) (200 A) shows a failure with a dimpled fracture surface, which occurred through the fusion zone and indicated a more ductile failure. In Figure 7(c) (225 A), failure occurred in the HAZ, which had been softened by recrystallization. The highest JBF was observed with this ductile HAZ failure mode.

D. *Hardness*

Hardness traverses along the top, middle, and bottom portions of the longitudinal sections of the crosswire joints are shown in Figure 8, for weld currents of 120, 150, and 225 A. The base metal hardness was in the range of 480 to 500 Hv, due to the cold drawing production process for fine wires, which typically creates a fine-grained unidirectional structure. Toward the weld, in the HAZ, elevated peak temperatures during the weld thermal cycle induced recrystallization of the fine-grained base metal (BM), resulting in a softened region.

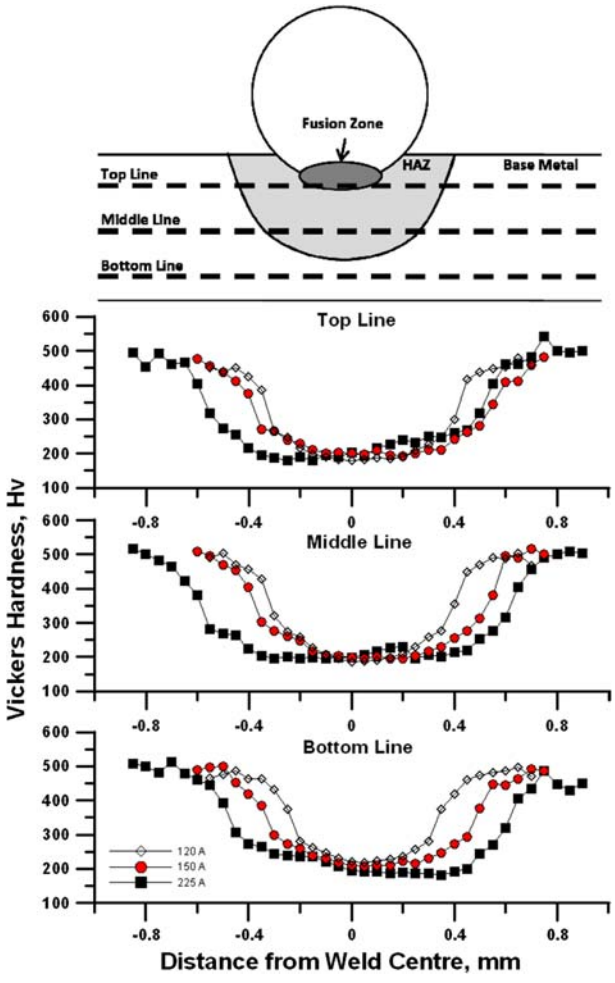

Fig. 8—Hardness trace along welded joint for welds made using 120 A and 1.5 kg-f weld force.

The softening effect increased approaching the weld centerline, as the peak temperatures increased as well. Other studies have shown similar softening in austenitic steels due to welding thermal cycles.[14,15]

From Figure 8, it can be shown that the size of the softened region increased with increasing current. Along with the softened region, the amount of set-down and HAZ depth also increased. For the 120 A condition, the general trend was a gradual decrease in HAZ size from the top to bottom profile, which corresponds with the expected peak temperature distribution. This result coincides with the interfacial failure mode, indicating fracture followed the softer region near the wire interface.

The 150 and 225 A welds produced a predominantly dendritic solidification structure near the faying surface. The minimum hardness values for all welds were near 200 Hv, and there was no apparent difference between the FZ and the HAZ. This was expected since there was a loss of the original work hardening due to recrystallization and resolidification of the austenitic microstructures in the HAZ and FZ, respectively. Furthermore, the enlarged softened regions of the higher current welds compared to the 120 A weld explain the transition from interfacial to partial interfacial failure mode.

A schematic depicting the fracture mode transition from interfacial to HAZ is shown in Figure 9. At lower currents, a weak bond induced interfacial failure. However, as the current increased, there was competition between interfacial and softened HAZ failure. Eventually, a transition occurred where fracture followed the softened HAZ/FZ region. Finally, during full set-down, fracture propagated through the soft outer edge of the HAZ material in one of the wires.

IV. DISCUSSION

A. *Mechanism of Joint Formation*

The mechanisms of joint formation of crossed RMW wire have been detailed by Fukumoto *et al.* for Ni, Au-plated Ni, and SUS304 SS.[5–7] Fukumoto and Zhou[5] showed a maximum JBF of around 70 N (~7 kg-f) for 400-μm-diameter Ni wire at 450 A. In a later publication, Fukumoto *et al.*[6] reported similar strengths for 400-μm Ni wire plated with 4-μm Au; however, a higher 600 A current was required for bonding. Recently, Fukumoto *et al.*[7] examined 400-μm-diameter SUS304 SS wire using an 8-ms weld time. It was determined that a JBF of about 120 N could be attained when employing a 6 kg-f welding force and 300 A current. Each of the aforementioned publications stated that the primary joining mechanism was solid-state bonding. In contrast, the current study showed that the primary mechanism observed for 316 LVM SS crossed-wire welding was fusion welding.

Figure 10 shows a schematic diagram detailing the joint formation for 316 LVM SS. During welding, the 1.5 kg-f welding force resulted in an initial deformation and larger contact area (Figures 2(a) and 10(a)). As the welding current increased to 90 A, surface material and

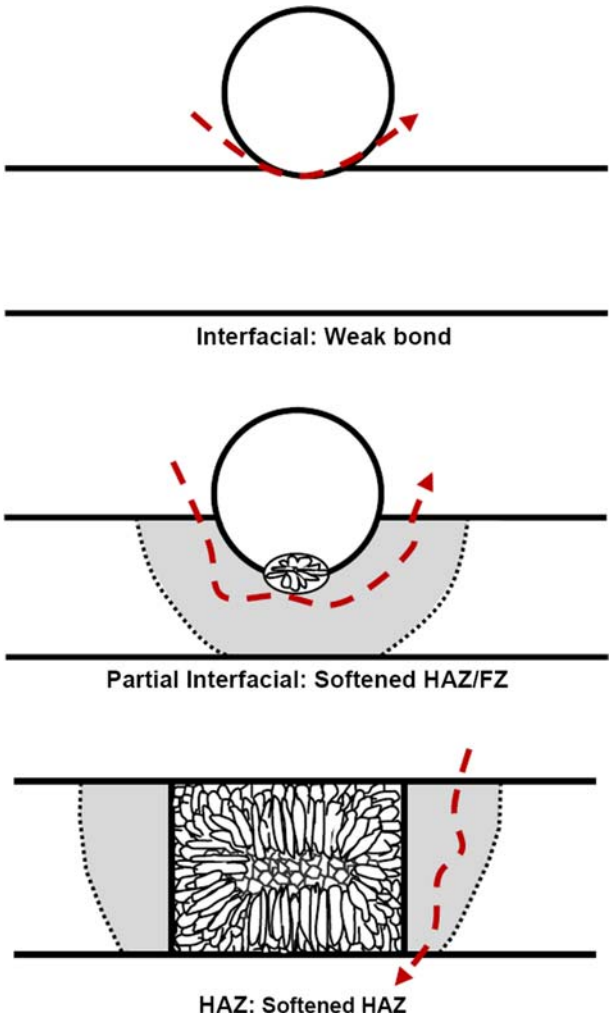

Fig. 9—Schematic of failure modes transitioning from interfacial to HAZ.

contaminants were melted and expelled from the interface. This expulsion aided in cleaning the interface by squeezing out contaminants (Figures 2(b), 2(c), 10(b), and 10(c)). Further increase in current resulted in a recrystallized HAZ and formation of a solid-state bond (Figures 2(d) and 10(d)). The recrystallized HAZ exhibited a lower hardness (200 Hv) compared to the fine-grained base metal (500 Hv) microstructure. During RMW of Ni wire, Fukomoto *et al.* observed both surface melting and recrystallization stages.[6]

As currents increased to 120 A, peak temperatures at the weld interface surpassed the liquidus temperature and generated a fusion zone (Figures 2(e) and 10(e)). The fusion zone was characterized by a columnar dendritic solidification structure surrounded by a recrystallized HAZ. At higher currents, the fusion zone growth was coupled with increased set-down and expulsion (Figures 2(f) and 10(f)). Full set-down was observed at 225 A with a predominately fusion-welded joint having a columnar dendritic structure (Figures 2(g) and 8(g)). Finally, overwelding occured when currents reached 350 A. Excessive heating caused severe expulsion and deformation, which adversely affected mechanical properties. Electrode sticking, however, was not observed at the current levels tested.

The differences in bonding mechanism compared to past literature may be attributed to several factors, including welding force, current, and material properties. For example, the lower electrical resistivity of Ni (69.3 $\mu\Omega$ mm) compared to 316LVM SS (740 $\mu\Omega$ mm) resulted in lower peak temperatures in Ni during RMW.[16,17] The higher peak temperatures for SS were more likely to surpass the liquidus temperature and form a fusion zone. However, SUS304 SS also produced a predominately solid-state bond, and it has similar electrical resistivity (720 $\mu\Omega$ mm) to the 316 LVM SS. This was likely due to the higher electrode force used to weld SUS304 SS, 6 kg-f for SUS304, compared to 1.5 kg-f, which resulted in a lower current density, contact resistance, and peak temperatures.

B. *Transition in Mechanism of Joint Formation*

Experimental verification was conducted to characterize the transition from solid-state bonding to fusion welding. The JBF as a function of current for 1.5 and 5 kg-f and the corresponding transition in mechanism of joint formation are shown in Figure 11. It can be shown that similar JBF values were attained for both welding conditions; however, the range over which solid-state bonding is prevalent was increased by using a higher electrode force. Figure 12 shows the weld cross section for the 300 and 400 A conditions. Fusion occurred when currents reached 400 A, which was higher than the 120 A observed for the 1.5 kg-f welding force. Figure 13 shows similar HAZ fracture modes for the predominately solid-state 5 kg-f welding force, which was also observed for the 1.5 kg-f condition.

A schematic showing the transition in mechanism of joint formation is shown in Figure 14. Differences in solid-state and fusion welding mechanisms are largely dependent on the peak temperatures and, hence, heat generation. Lower force coupled with materials with high resistivity will tend toward fusion welding as compared to solid state, which requires higher force and lower material resistivity. It is well known that the approximate heat generated during RMW is constituted by the following equation:

$$Q = I^2 Rt \qquad [2]$$

where the current (I) and time (t) are controlled variables. The term R is the resistance, and in RMW, it is dependent on welding force and a combination of bulk resistivity and contact resistivity to give the overall material resistivity. Bulk resistance is a material property, while contact resistance generally decreases with increasing weld force. Referring to Figure 14, it can be shown that increasing welding force and lowering the overall resistivity generally tends toward decreased interfacial heat generation, which is ideal for solid-state bonding (shifts the transition toward higher currents). In contrast, lower welding force coupled with higher material resistivity creates a propensity toward fusion welding (shifts the transition toward lower currents).

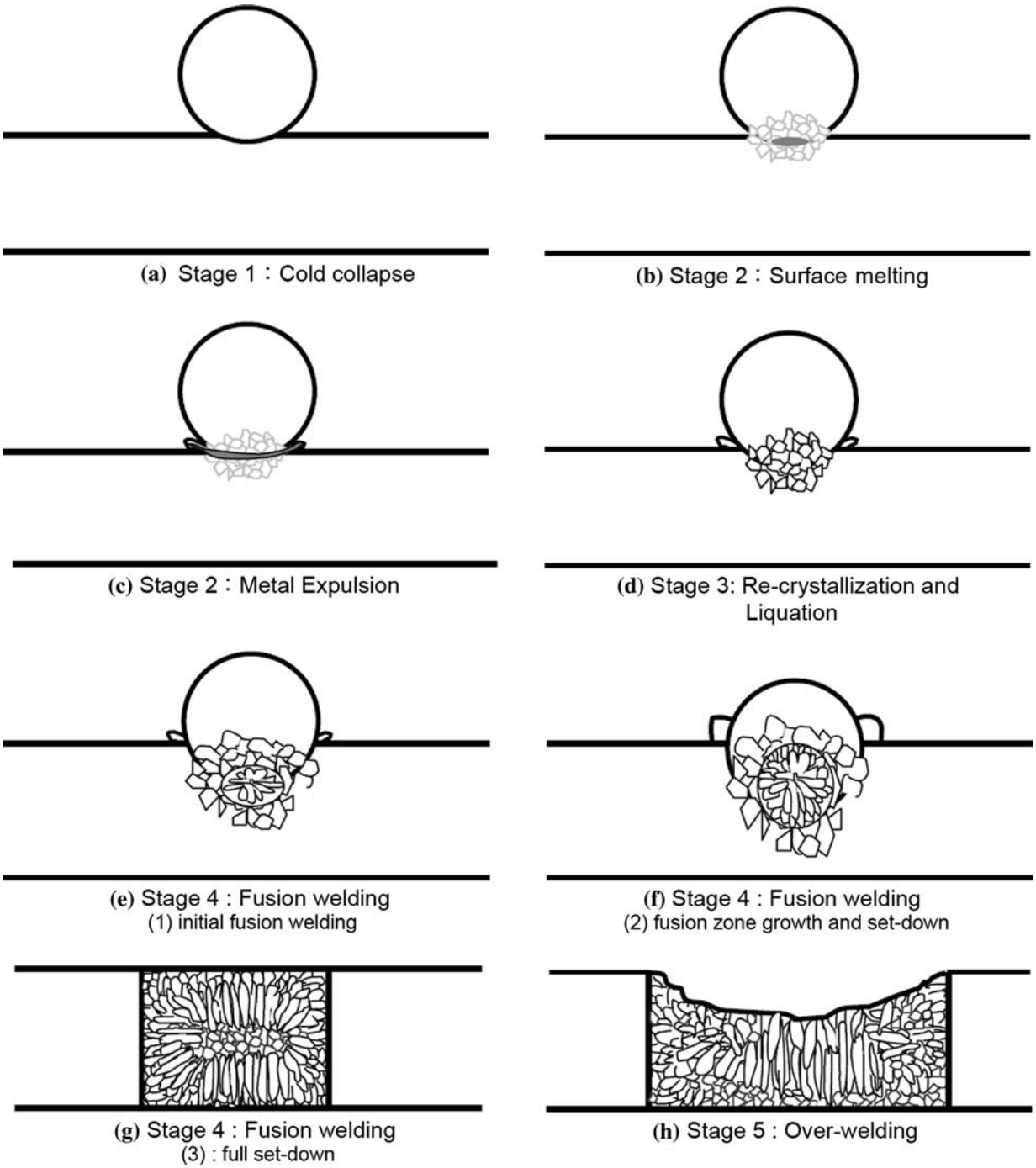

Fig. 10—Schematic of proposed RMW bonding mechanism of crossed 316 LVM SS wire.

Therefore, depending on the specific bonding condition and material properties, the resultant bonding mechanisms could be either solid state or fusion welding.

The JBF of the solid-state-bonded SUS304 SS was reported to be slightly higher than the 316 LVM in the current study. Discrepancies may be attributed to a combination of differences in wire diameter and base material tensile strength. Base metal strengths for the SUS304 SS are typically higher than the 316LVM SS; however, the 316 LVM SS has superior resistance to corrosion. In medical applications, such as stents, smooth surfaces are also critical in avoiding damage to the epithelial surface. Figure 15 shows the surfaces of the optimized JBF bonding condition for 304 and 316 LVM SS welded at fusion welding and solid-state bonding conditions, respectively. A smoother weld surface is observed for the fusion-welded 316 LVM compared to both solid-state welded 316 LVM and SUS304 SS, which exhibits rough flash material along the wire perimeter. This shows that the fusion-welded SS produced a smoother surface then the comparable joint using a solid-state bonding mechanism.

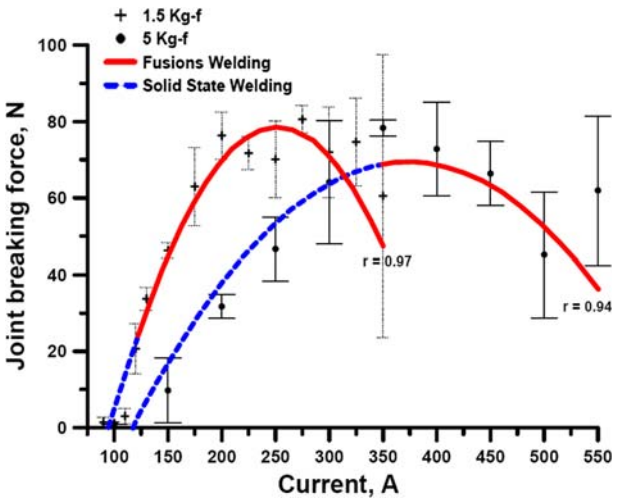

Fig. 11—JBF as a function of current for RMW 316 LVM.

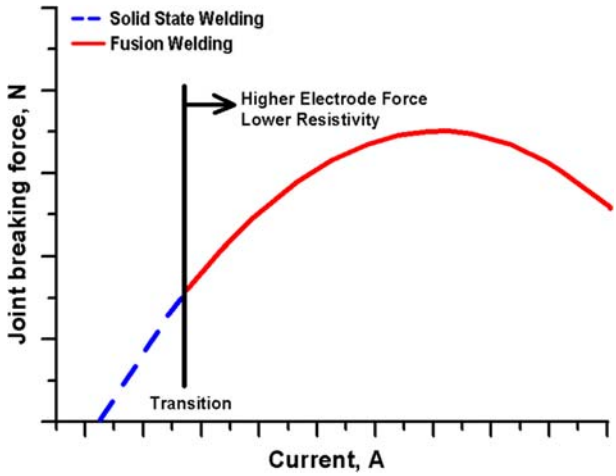

Fig. 14—Schematic showing transition in mechanism of joint formation.

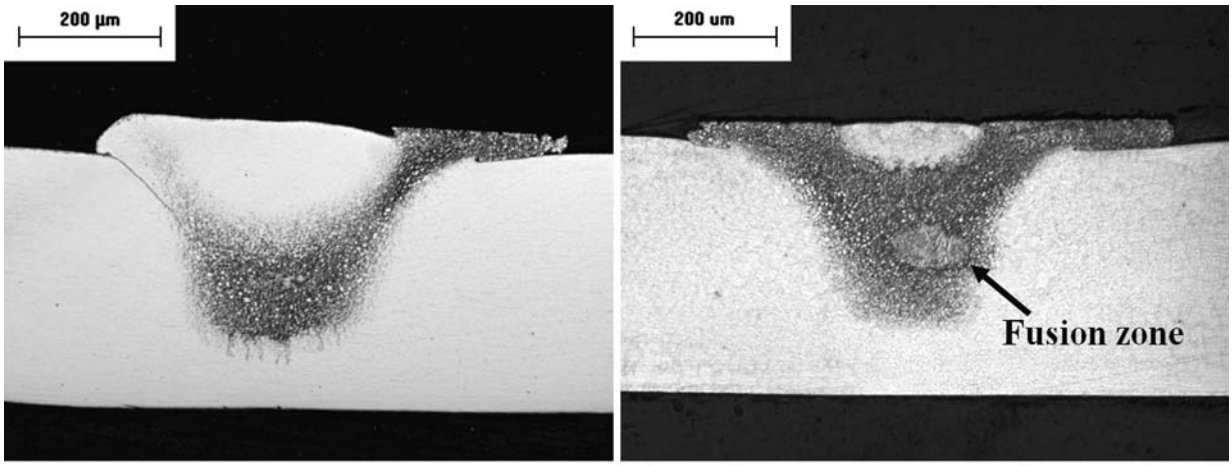

Fig. 12—Weld cross section for RMW made using 5 kg-f welding force.

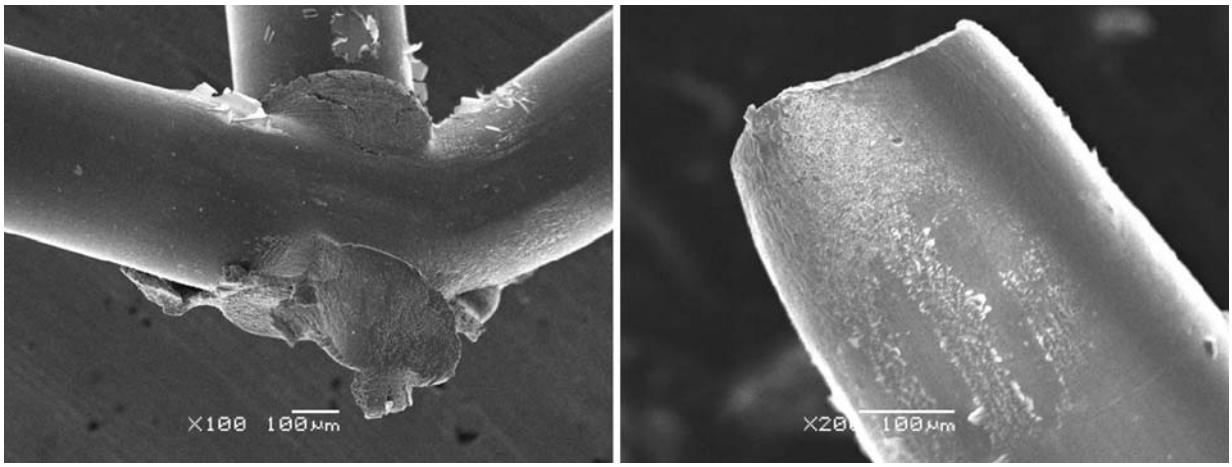

Fig. 13—Representative fracture surfaces for tensile test of 400 A and 5 kg-f weld.

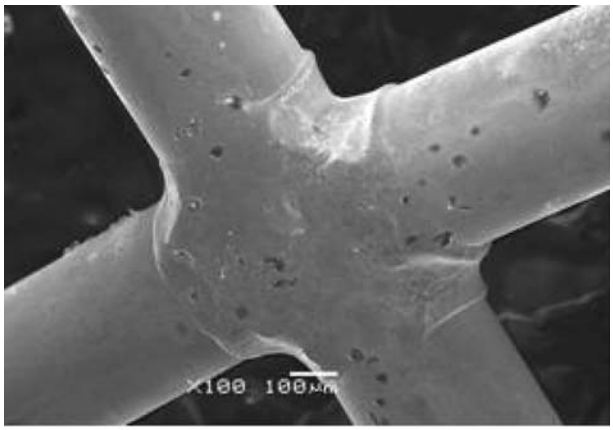

(a) 316LVM using 1.5 kg-f

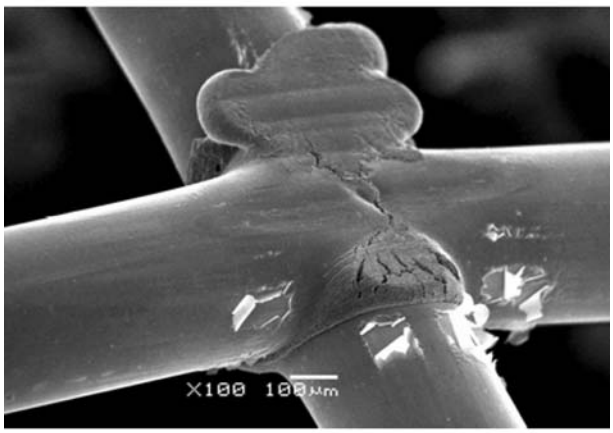

(b) 316LVM using 5 kg-f

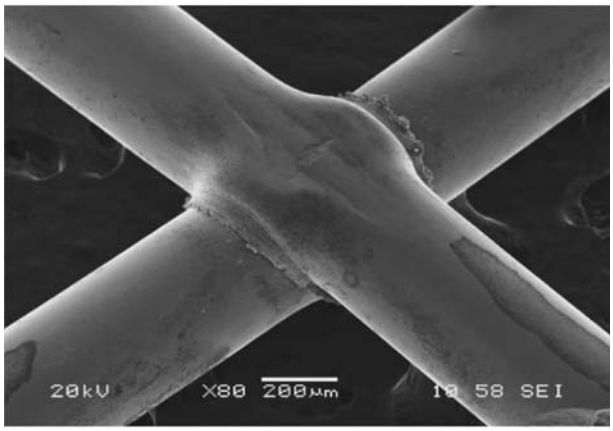

(c) 304 SS using 6 kg-f

Fig. 15—Surface of the optimized bonding condition for austenitic SS.

V. CONCLUSIONS

The present study has examined RMW of crossed 316 LVM SS wire by observing microstructure, mechanical properties, and fracture surfaces. The bonding mechanism was detailed and compared to Ni, Au-plated Ni, and SUS304 SS. In addition, the transition in the mechanism of joint formation was detailed. Key conclusions formed from the results and discussions are presented as follows.

1. The proposed bonding process is (1) cold collapse, (2) surface melting and squeeze-out, (3) recrystallization and liquation, (4) fusion welding, and (5) overwelding.
2. Solid-state bonding transitioned to fusion welding, and the tendency for fusion welding was promoted with both increased material resistivity and lowered welding force. Fusion welding stages include (a) initial fusion welding, (b) fusion zone growth and set-down, and (c) full set-down, sequentially.
3. Fracture modes in tensile testing progressed with increasing current from interfacial failure to fusion zone failure and, finally, to HAZ failure.
4. The JBF and set-down increased with increasing weld current, reaching a maximum JBF of 8 kg-f with 100 pct set-down.
5. Fusion welding at low bonding force (1.5 kg-f) resulted in sound joints with smooth surfaces and high JBF.

REFERENCES

1. S. Fukumoto, T. Matsuo, H. Tsubakino, and A. Yamamoto: *Mater. Trans.*, 2007, vol. 48 (4), pp. 813–20.
2. R. Singh and N.B. Dahotre: *J. Mater. Sci.*, 2005, vol. 40 (21), pp. 5619–26.
3. D.R. Haynes, T.N. Crotti, and M.R. Haywood: *J. Biomed. Mater. Res.*, 2000, vol. 49 (2), pp. 167–75.
4. I. Khan and Y. Zhou: *Proc. in Materials and Processes for Medical Devices Conf. (MPMD)*, Palm Springs, CA, Sept. 2007.
5. K.J. Ely and Y. Zhou: *Sci. Technol. Weld. Join.*, 2001, vol. 6 (2), pp. 63–72.
6. W. Tan, Y. Zhou, and H.W. Kerr: *Metall. Mater. Trans. A*, 2002, vol. 33A, pp. 2667–76.
7. S. Fukumoto and Y. Zhou: *Metall. Mater. Trans. A*, 2004, vol. 35A, pp. 3165–76.
8. S. Fukumoto, Z. Chen, and Y. Zhou: *Metall. Mater. Trans. A*, 2005, vol. 36A, pp. 2717–24.
9. V.E. Ataush, E.G. Moskvin, and V.P. Leonov: *Weld. Int.*, 1992, vol. 6 (8), pp. 624–27.
10. C.D. Lundin, C.Y.P. Qiao, and Y. Kikuchi: *Heat-Resistant Materials*, Proc. 1st Int. Conf., ASM International, Fontana, WI, 1991, pp. 71–79.
11. J.C. Lippold and D.J. Kotecki: *Welding Metallurgy and Weldability of the Stainless Steels*, John Wiley & Sons, Inc., Toronto, ON, Canada, 2005, pp. 153 and 155.
12. V.P. Kujanpaa, S.A. David, and C.L. White: *Weld. J.*, 1987, vol. 66 (8), pp. 221–28.
13. A. Wang, O. Ohashi, N. Yamaguchi, M. Aoki, Y. Higashi, and N. Hitomi: *Nucl. Instrum. Meth. Phys. Res., Sec. B: Beam Interact. Mater. Atoms*, 2003, vol. 206, pp. 219–23.
14. K. Tsuchiya, H. Kawamura, and G. Kalinin: *J. Nucl. Mater.*, 2000, vol. 283 (287), pp. 1210–14.
15. B. Gulenc, K. Develi, N. Kahraman, and A. Durgutlu: *Int. J. Hydrogen Energy*, 2005, vol. 30, pp. 1475–81.
16. http://www.allmeasures.com/Formulae/static/materials/24/electrical_resistivity.htm.
17. http://www.lenntech.com/Stainless-steel-316L.htm.